Two-photon fluorescence isotropic-single-objective microscopy

Eric Le Moal, Emeric Mudry, Patrick C. Chaumet, Patrick Ferrand, and Anne Sentenac*

Institut Fresnel, CNRS, Aix-Marseille Université, Ecole Centrale Marseille, Campus de St. Jérôme, 13013 Marseille, France
Corresponding author: anne.sentenac@fresnel.fr

Two-photon excitation provides efficient optical sectioning in three-dimensional fluorescence microscopy, independently of a confocal detection. In two-photon laser-scanning microscopy, the image resolution is governed by the volume of the excitation light spot, which is obtained by focusing the incident laser beam through the objective lens of the microscope. The light spot being strongly elongated along the optical axis, the axial resolution is much lower than the transverse one. In this Letter we show that it is possible to strongly reduce the axial size of the excitation spot by shaping the incident beam and using a mirror in place of a standard glass slide to support the sample. Provided that the contribution of sidelobes can be removed through deconvolution procedures, this approach should allow us to achieve similar axial and lateral resolution.   © 2011 Optical Society of America

OCIS Codes: 180.2520, 180.4315, 180.6900.

Confocal laser-scanning fluorescence microscopy (CLSM) and two-photon laser-scanning fluorescence microscopy (2PFM) have been widely developed, notably in life sciences, due to their capacity of optical sectioning that allows three-dimensional (3D) imaging [1,2]. While optical sectioning in CLSM is obtained through light rejection from out-of-focus parts by spatial filtering, 2PFM exhibits intrinsic optical sectioning due to its nonlinear absorption process. However, both CLSM and 2PFM suffer from a strongly anisotropic resolution due to the elongated shape of their excitation and detection point-spread function (PSF) along the lens axis [1]. In the best case, the axial resolution is about threefold lower than the transverse one.

The resolution anisotropy stems fundamentally from the asymmetry of the microscope. With a single objective lens, light is focused and collected from only one side of the sample. The missing illumination and observation directions are responsible for the rice-grain-shaped PSF. To obtain a quasi-isotropic resolution, the sample should be illuminated and observed from all possible directions. This configuration is almost reached in the 4Pi microscope where the sample is sandwiched between two objective lenses facing each other [3]. Simultaneous focusing of a laser beam through these two objective lenses yields an interference pattern that exhibits a quasi-isotropic light spot flanked by multiple sidelobes. These sidelobes result from the limited NA of the objective lenses, namely the missing light at the higher angles of incidence (the smaller the NA, the higher the sidelobes). Two-photon excitation [4] can be used to decrease the amplitude of the sidelobes. Combined with a confocal detection [5] and a simple deconvolution algorithm [6], this technique yields spectacular 3D images with an axial resolution similar to the transverse one [5–7]. However, its implementation, which requires a very careful tuning of the two objective lenses, remains difficult to adapt in routine applications.

Recently, we have shown that a quasi-isotropic spot, similar to that obtained in a 4Pi microscope, can be formed with a single objective lens [8,9]. The idea consists in placing a mirror after the lens and shaping the illumination beam so that both the incident and reflected fields converge toward the same point. Practically, the beam is shaped by a spatial light modulator (SLM) so that it focuses at two points along the optical axis. The mirror is simply placed at equidistance between these two points. The resulting quasi-isotropic spot formed above the mirror is axially moved by changing the distance between the two points. Using a confocal detection and single-photon excitation, we obtained a PSF similar to that of a 4Pi microscope of type A [8,9]. In this Letter, we show that this concept can be adapted to 2PFM, and we demonstrate a fourfold to fivefold reduction of the excitation spot axial width.

Our experimental setup (see Fig. 1) is based on a standard inverted fluorescence microscope equipped with a pulsed laser source (Nd-YVO$_4$, Amplitude) emitting 6 ps pulses at 1064 nm with a repetition rate of 34.5 MHz. We
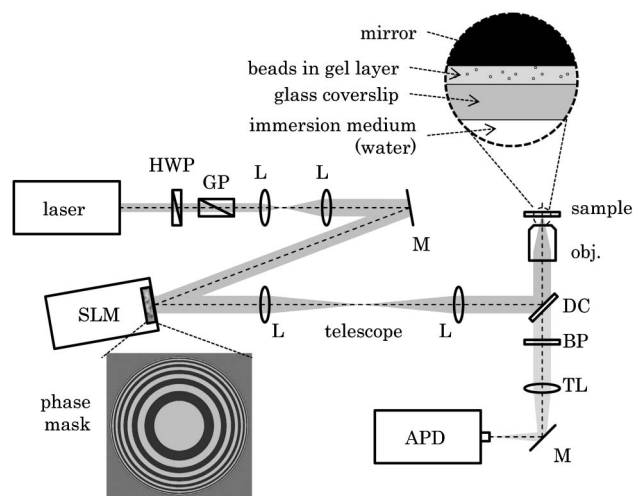

Fig. 1.   Schematic view of our experimental two-photon fluorescence isotropic-single-objective microscopy setup. (Inset) Typical phase mask for isotropic focusing at 6 μm above the reflective substrate. HWP, half-wave plate; GP, Glan prism; L, achromatic doublet; M, mirror; obj., objective; DC, dichroic beam splitter; BP, bandpass filter; TL, microscope tube lens; APD, avalanche-photodiode photon counter. See text for details.

used a water-immersion objective lens (Plan Apo VC 60X, Nikon) of NA 1.20. The fluorescence light was collected in epi-geometry, spectrally filtered using a dichroic beam splitter (645DCSP45°, Chroma) and a bandpass emission filter (HQ540/80M-2P, Chroma) and detected, without any spatial filtering, by a single-photon avalanche diode (Micro Photon Devices) adapted to the camera port of the microscope. The collimated laser beam was shaped by a phase-only SLM (X8267-15, Hamamatsu) placed in a plane optically conjugated to the rear focal plane of the objective lens. In this plane, the beam field was linearly polarized along the x axis (which corresponded to the active axis of the SLM). Transverse scanning was performed by moving the sample with a nanopositioning stage (NanoLP100, MadCity Labs), while axial scanning was performed by displaying different phase masks on the SLM. Details of phase mask design and calibration can be found in [9]. Note that the transverse scan could be done without moving the sample by tilting the incident beam with galvanometric mirrors (like in a standard confocal microscope).

Following [9], we first simulated the microscope performances. Without any spatial filtering of the fluorescence, the resolution of the image is given directly by the size of the excitation spot. The incident field illuminating the mirror is cast as a sum of 500×180 plane waves with regular spacing in polar and azimuthal angles within the angular aperture of the objective lens and appropriate polarization and amplitude [10]. The phase of each plane wave is fixed by the phase mask displayed on the SLM (one example is given in Fig. 1) [8,9]. To generate two spots at z_0 and $-z_0$ with respect to the focal plane, the phase mask value displayed at distance ρ from the optical axis reads $f(\rho) = \Pi/2 \, \text{sign}[\sin(z_0 k_0 \cos\theta)]$, where ρ is related to the incidence polar angle θ through $\sin\theta \propto \rho$ (Abbe sine condition) and k_0 is the wavenumber in the sample medium. In our configuration, the total PSF of the microscope is given by $|\mathbf{E}_{tot}(\mathbf{r})|^4$, where $\mathbf{E}_{tot}$ is the sum of the incident and mirror reflected field. For comparison purposes, the PSF of standard nonconfocal

Table 1. Specifications of PSFs

	FWHM (μm)[a]		
	z	y	x
2PFM$_{th}$	0.92	0.42	0.32
ISO-2PFM$_{th}$	0.18	0.35	0.32
2PFM$_{exp}$	1.11	0.47	0.36
ISO-2PFM$_{exp}$	0.25	0.40	0.36
Relative Intensity of First Sidelobes			
ISO-2PFM$_{th}$	40%		
ISO-2PFM$_{exp}$	55%–60%		

[a]For ISO-2PFM, widths of central lobe are given.

2PFM is also simulated. Axial and transverse views of these PSFs are shown in Fig. 2a, and their main characteristics are reported in Table 1. Using an objective lens with NA = 1.2 in water, the isotropic-single-objective microscopy (ISO-2PFM) exhibits a quasi-isotropic central spot flanked by sidelobes of relative amplitude 40%. Similar to the 4Pi illumination scheme, the transverse extension of the PSF is 15% smaller than that of the standard 2PFM in the direction orthogonal to the field polarization in the SLM plane (y axis).

The experimental PSFs were obtained by measuring the 3D images of isolated subwavelength beads. For ISO-2PFM, the sample consisted of 200 nm spheres (Fluospheres Orange 540/560 nm, Invitrogen) spread in a 10 μm thick layer of 1 wt.% agarose gel mounted between a silver mirror and a conventional glass coverslip. This mounting was repeated for 2PFM with a microscope glass slide instead of the mirror. Axial and transverse slices taken from these 3D images are shown in Fig. 2b. Assuming that a 200 nm sphere is almost a point object upon illumination at 1064 nm, these data indicate that the axial width of the PSF in ISO-2PFM is four to five times smaller than that in 2PFM. Figure 3 shows the intensity profiles along the z axis, across the center of one bead image, for ISO-2PFM and 2PFM. Similar to the simulations, the experimental axial profile of the PSF in ISO-2PFM is almost perfectly contained in the experimental profile of the PSF in 2PFM.
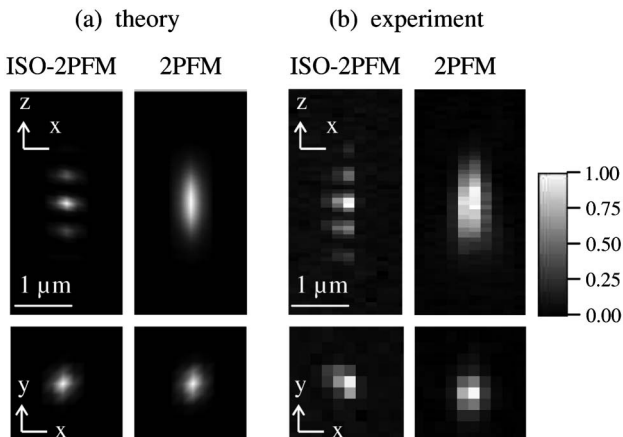
(a) theory (b) experiment

Fig. 2.   Axial (zx) and transverse (xy) views of (a) the theoretical PSF in ISO-2PFM and standard 2PFM and (b) 3D fluorescence images of 200 nm beads experimentally measured by ISO-2PFM and standard 2PFM. Both microscopy techniques are based on nonconfocal detection. Images are displayed with a linear gray-level scale.
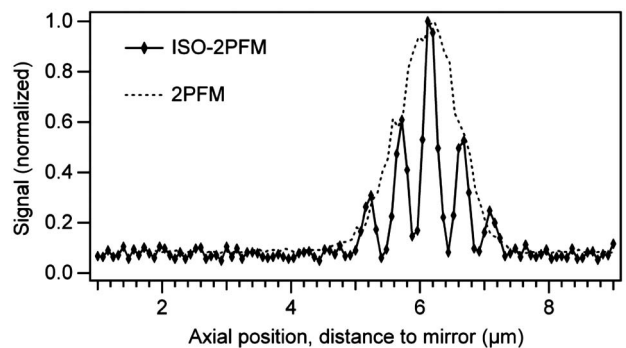

Fig. 3.   Intensity profile measured along the z axis on 3D fluorescence images of 200 nm beads [see Fig. 2b] by ISO-2PFM (solid line) and standard 2PFM (dashed line). The origin of the bottom axis corresponds for ISO-2PFM to the position of the mirror surface.

The small discrepancies between the theoretical and experimental PSFs are essentially due to the imperfect apodization function of the objective lens that attenuates the amplitude of the plane waves at high polar angles more quickly than the standard radiometric coefficient $(\cos\theta)^{0.5}$ [11]. This directly affects the axial width of the 2PFM PSF, which appears larger than the theoretical one. As a result, the relative intensity of the sidelobes of the experimental ISO-2PFM PSF are also higher (55% to 60%) than expected (40%). To improve this point, the apodization function could be compensated for by adding an amplitude mask at the rear pupil of the objective lens. Without confocal detection, the sidelobes remain higher in relative intensity than those in a 4Pi confocal microscope of type A; however, they are lower than those in I^5M [6]. Hence, as it stands, the microscope should allow imaging 3D samples provided that iterative deconvolution procedures, similar to those used in I^5M, are employed to process the data [5].

Now we discuss the main limitations of ISO-2PFM and solutions to overcome them. First, the available range of axial scanning in ISO-2PFM is dependent on the SLM features. Increasing the distance between the two spots at z_0 and $-z_0$ requires higher spatial frequencies in the phase mask, which may not be properly displayed if they overstep the SLM resolution. In our setup, the available scanning range was estimated to about 15 μm, based on the observation of moiré beating in the phase masks for larger z_0. This limit can be pushed back by using SLMs of higher resolution. When using femtosecond laser pulses, short coherence length can also be a limit to the available range of axial scanning. Assuming that coherence length is only limited by pulse duration, 300 fs pulses would typically allow scanning up to $z_0 = 30$ μm. Hence, a trade-off has to be found between excitation efficiency and scanning range. Besides, the chosen mask design also imposes a lower bound to the scanning range, beyond which two spots do not distinctly form at z_0 and $-z_0$. This directly ensues from the simplification of the wavefront with a binary function. As the spot forms closer to the mirror, that binary function tends to a constant function; hence, it results in a spot forming at the median plane. As a loose criterion, scanning is possible down to $z_0 = \lambda$, with λ the excitation wavelength in sample medium (here $\lambda \sim 0.8$ μm). When this lower bound is problematic for imaging thin samples, one solution consists in depositing a transparent layer of at least this thickness and refractive index close to that of the sample on the mirror. On the other hand, we recently proposed a different mask design based on (not binary) Fresnel-lens masks that, in principle, allows scanning down to $z_0 = 0$ with no artifact and almost the same efficiency [9]. As a last remark, 4Pi and ISO microscopy are subject to the same PSF distortions when light propagates through inhomogeneous samples, except that the reflection in the mirror makes the light path in the sample twice as long in ISO as in 4Pi microscopy. Nevertheless, iterative deconvolution

techniques have previously been developed for 4Pi microscopy to restore altered images of the specimen with strong variations of refractive index [12], which can similarly be applied to ISO microscopy.

In conclusion, we believe that ISO-2PFM is an elegant solution to ameliorate the axial resolution of two-photon scanning microscopy. It is simple to implement and very stable, as the scanning can in principle be performed in the three directions without moving the sample (when using galvanometric mirrors). Another advantage is that ISO-2PFM does not require as high illumination power as 2PFM since the reflective substrate brings about a four-fold increase in the incident peak intensity and almost doubles the collection efficiency. Hence out-of-focus photobleaching and photodamage are further reduced. Moreover, the reflective substrate makes possible the detection of both backward and forward emitted light; hence, this arrangement suits the detection of coherent emission processes like second harmonic generation (SHG). An important improvement of the technique would be to implement confocal detection. This could be achieved by adding a second SLM adapted to the fluorescence wavelength. In principle, such a detection scheme would yield the same PSF as that of a confocal 4Pi microscope of type A with two-photon fluorescence and that of type C with SHG.

References

1. A. Diaspro, ed., *Confocal and Two-Photon Microscopy* (Wiley-Liss, 2001).
2. J. Pawley, ed., *Handbook of Biological Confocal Microscopy* (Springer, 2006).
3. S. W. Hell and E. H. K. Stelzer, J. Opt. Soc. Am. A **9**, 2159 (1992).
4. S. W. Hell and E. H. K. Stelzer, Opt. Commun. **93**, 277 (1992).
5. J. Bewersdorf, R. Schmidt, and S. W. Hell, J. Microsc. **222**, 105 (2006).
6. M. G. L. Gustafsson, D. A. Agard, and J. W. Sedat, J. Microsc. **195**, 10 (1999).
7. H. Gugel, J. Bewersdorf, S. Jakobs, J. Engelhardt, R. Storz, and S. W. Hell, Biophys. J. **87**, 4146 (2004).
8. E. Mudry, E. Le Moal, P. Ferrand, P. C. Chaumet, and A. Sentenac, Phys. Rev. Lett. **105**, 203903 (2010).
9. E. Le Moal, E. Mudry, P. C. Chaumet, P. Ferrand, and A. Sentenac, J. Opt. Soc. Am. A **28**, 1586 (2011).
10. P. Török, P. D. Higdon, and T. Wilson, Opt. Commun. **148**, 300 (1998).
11. H. J. Matthews, D. K. Hamilton, and C. J. R. Sheppard, J. Mod. Opt. **36**, 233 (1989).
12. G. Vicidomini, R. Schmidt, A. Egner, S. W. Hell, and A. Schönle, Opt. Express **18**, 10154 (2010).